Hindawi
Science and Technology of Nuclear Installations
Volume 2022, Article ID 3563459, 14 pages
https://doi.org/10.1155/2022/3563459

Research Article

Pressure Distribution on the Inner Wall of the Volute Casing of a Centrifugal Pump

Yu-Liang Zhang,[1] **Jin-Fu Li**,[2] **Tao Wang**,[1] **Jun-Jian Xiao**,[1] **Xiao-Qi Jia**,[3] **and Li Zhang**[4]

[1]*College of Mechanical Engineering & Key Laboratory of Air-driven Equipment Technology of Zhejiang Province, Quzhou University, Quzhou 324000, China*
[2]*College of Mechanical Engineering, Zhejiang University of Technology, Hangzhou 310023, China*
[3]*The Zhejiang Provincial Key Lab of Fluid Transmission Technology, Zhejiang Sci-Tech University, Hangzhou 310018, China*
[4]*Department of Application & Engineering, Zhejiang Institute of Economics and Trade, Hangzhou 310018, China*

Correspondence should be addressed to Tao Wang; wtcat@163.com

Received 10 January 2022; Revised 16 April 2022; Accepted 27 April 2022; Published 19 May 2022

Academic Editor: Iztok Tiselj

In order to grasp the distribution characteristics of the pressure field on the inner wall of the volute casing of an atypical open impeller centrifugal pump, the instantaneous pressure at different operating conditions was experimentally measured under four operating rotational speeds to obtain the distribution characteristics of the average static pressure field in the volute casing of this pump model. The pressure pulsation amplitude and pressure pulsation intensity were also analyzed at different rotational speed cases, and the standard deviation analysis was performed. The results showed that the instantaneous pressure pulsation on the inner wall of the volute casing strongly fluctuates during the pump operating, and the closer to the volute casing outlet, the more intense the pressure pulsation was. After increasing the pump shaft speed, the fluctuation amplitude gradually decreased. The pressure pulsation on the wall of tip clearance is more intense than that on the inner wall of the volute shell. The intensity of the pressure pulsation on the wall of tip clearance decreases with the increase of the rotational speed, and the higher the speed, the less intense the pressure pulsation.

1. Introduction

As one of the most widely used rotating machines, centrifugal pumps play a very important role in nuclear power, petrochemical, and other applications. As one of the main flow parts of centrifugal pumps, the hydraulic characteristics of the volute casing play a crucial role in the efficiency of centrifugal pumps. The pressure pulsation of the centrifugal pump is an important factor in the vibration and noise of the pump unit due to the rotor-stator interaction between the rotational impeller and the static volute casing [1]. Therefore, it is important to master the pressure field characteristics of centrifugal pumps in different operating conditions of flow components to improve the operational reliability of centrifugal pumps.

In past years, many scholars have tried to master the internal pressure fluctuation characteristics. Spence et al. studied the pressure pulsation of fifteen pressure measurement points to investigate the location of the most intense pulsation of pressure changes inside the centrifugal pump [2]. Parrondo-Gayo et al. measured the pressure pulsation inside the discharge chamber of a centrifugal pump and found that the magnitude of the pressure pulsation mainly depends on the intensity of the rotor-stator interaction [3]. Khalifa et al. found that the radial clearance between impeller and volute tongue of a double suction centrifugal pump could cause strong pressure pulsation near volute tongue [4]. Wang et al. concluded that the pressure pulsation of its main frequency appeared at the nondesign point and at the multiplication of the vane frequency [5]. Yao et al. found that the pressure fluctuations of the impeller rotation frequency dominated in the semispiral suction chamber [6]. Wang et al. found that the pressure pulsation at the top of the semispiral suction chamber at low flow rate

existed due to the harmonics of the third axial frequency caused by the impeller rotation stall, and the pressure pulsation decreased and then increased as the rotational speed decreased [7]. Zheng et al. found that the gap flow rate has a significant effect on the pressure fluctuation of centrifugal pumps, and the amplitude of the main frequency of the impeller inlet pressure fluctuation increases with the increase of the flow rate [8]. Zhang et al. found that the slanting volute gear has a significant effect on reducing the pressure pulsation [9]. Zhang et al. analyzed the frequency spectrum of the pressure pulsation signal at different flow rates and studied the relative velocity distribution inside the vane channel to clarify the correlation between the flow structure and the pressure spectrum [10].

Zhang et al. found that there was no obvious peak signal induced by nonlinear interference between the axial frequency and its lobe frequency in the pressure spectrum [11]. Yao et al. summarized the universal pressure pulsation measurement points, sampling frequency, sampling duration, and the selection method of fast Fourier transform [12]. Zhao et al. found that the interaction between the stall unit and the spacer tongue may lead to rotor-stator interaction [13]. Wang et al. found that the pressure pulsation at the spacer tongue was the main noise source and resonated with the volute housing [14]. Chen et al. found that the pressure pulsation at the spacer tongue was the main noise source and resonated with the volute casing, and found that the coupling between the impeller outlet and the volute casing is the main influencing factor of the pressure pulsation in the volute casing [15]. Yuan et al. found that with the increase of flow rate, the relative velocity in the impeller increases significantly, which has a direct impact on the performance of centrifugal pumps with diverging vane [16]. Shi et al. found that at the same flow rate, the smaller the clearance, the more intense the pressure pulsation [17], and the larger the amplitude of pulsation at the main frequency, at the same flow rate, the average value of radial force increases for both increasing or decreasing clearance. The transient unstable flow in nuclear coolant pumps [18–24] and more pressure pulsation inside pumps [25–31] are also deeply studied.

It is seen from above studies the pressure monitors in these models are relative insufficient. Therefore, in order to grasp the transient flow characteristics inside the pump more comprehensively, this paper tests the static pressure distribution at different radii on the solid wall surface of the volute casing of a model atypical open impeller centrifugal pump according to the transient performance test bench of the pressure field inside the centrifugal pump, and also compares the pressure pulsation amplitude and pressure pulsation intensity under different speed cases, and conducts the standard deviation analysis. The pressure distribution characteristics of the inner wall surface of the volute casing of this model pump are well revealed.

2. Test Rig and Physical Pump

2.1. Tested Pump. The model pump to be tested is a low specific speed centrifugal pump, and the volute casing and the assembly relationship with the impeller are shown in Figures 1 and 2. The design parameters are as follows: flow rate $Q = 6\ m^3/h$, head $H = 8$ m, and speed $n = 1450$ r/min. The pump inlet and outlet diameters are 50 mm and 40 mm, respectively. The pump has five double-arc cylindrical vanes with 1.2 mm top clearance and 160 mm impeller diameter. The volute casing size variation law is in the form of Archimedean spiral, and the pole diameter $d = 82.5 + (15\theta)/360$ mm, where θ is the angle of the circle center from the eighth section. The detailed geometric parameters of the test pump are presented in the literature [32, 33].

2.2. Test System of Pressure Field. The model of centrifugal pump pressure field test system is shown in Figure 3. The fluid inside the pump body is introduced into the multichannel pressure sensor integrated device through a slender tube, as shown in Figures 4 and 5, and with the help of the pressure sensor, the pressure magnitude signal is obtained and converted into an electrical signal and input to the computer to complete the data acquisition and processing. In this experiment, it is necessary to measure the circumferential direction of the volute casing midsection, the $D = 100$ mm and $D = 140$ mm circumferential directions on the solid wall surface of the lobe top clearance.

The centrifugal pump unit consists of an electric motor, a torque speed sensor, and the centrifugal pump to be tested, as shown in Figure 3. The driving motor is a 4.0 kW three-phase AC motor. A frequency converter (MICROMASTER 440 manufactured by SIEMENS) was used to adjust the pump rotational speed. An NJ1 torque detector with a range of 0–50 N·m was employed to measure the instantaneous rotational speed and torque with the total uncertainty of ±0.93% and an accuracy rating of 0.5. An electromagnetic flowmeter (OPTIFLUX2100C) with a range of $0–30\ m^3/h$ was utilized to measure the instantaneous flow rate with an uncertainty of ±0.5% and an accuracy rating of 0.5.

2.3. Pressure Measurement Point Arrangement. In this paper, the pressure measurement points on the inner surface of the volute casing are located in the circumferential direction of the volute casing in the cross-section and the solid wall surface of the lobe top gap, with a total of 15 pressure measurement points in the former and 30 pressure measurement points in the latter, all of which are instantaneous static pressure measurement, and the range of the pressure sensor is −0.1 to +1 MPa.

The location of the pressure measurement points in the volute casing of the centrifugal pump is shown in Figure 6, and the geometric coordinates of the circumferential pressure measurement points in the volute casing are shown in Table 1. The arrangement scheme of the pressure measurement points on the solid wall surface of the lobe top clearance is 15 points on each radius inside and outside the radius, and the angular distance between adjacent measurement points at the same radius is 24°. The inner circle radius is $D = 100$ mm, and the outer circle radius is $D = 140$ mm.

During the experiment, the corresponding stable speed and stable flow condition point are obtained by adjusting the inverter and outlet valve. The free liquid level of the tank is

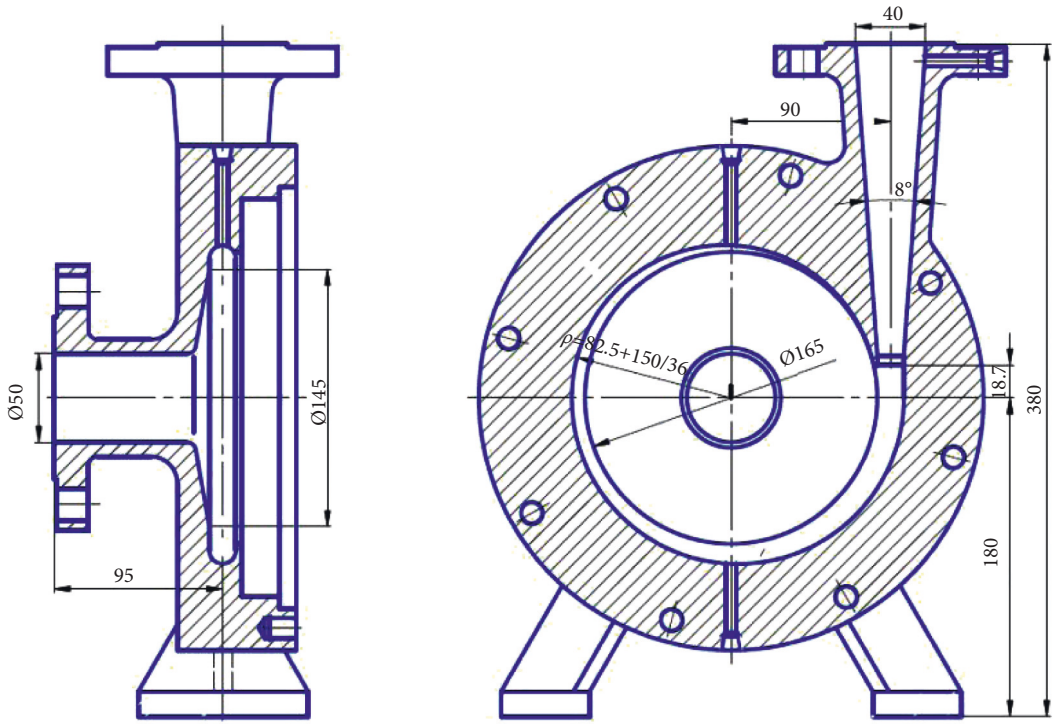

Figure 1: Pump volute.

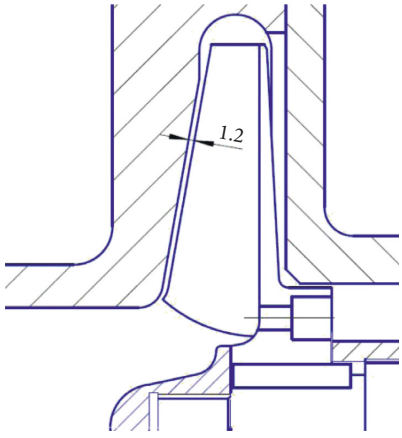

Figure 2: Tip clearance.

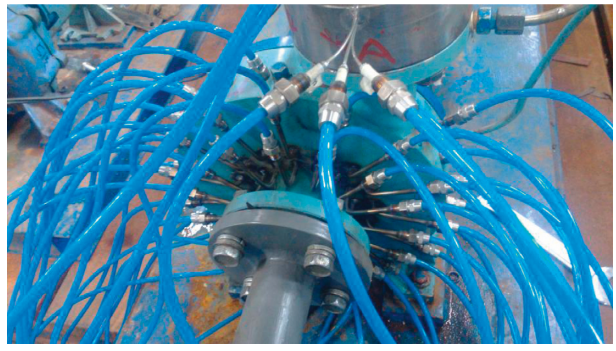

Figure 4: Pressure test unit of centrifugal pump.

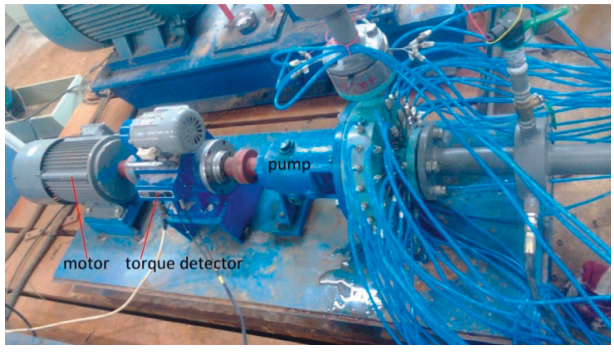

Figure 3: The test unit of pressure field of centrifugal pump.

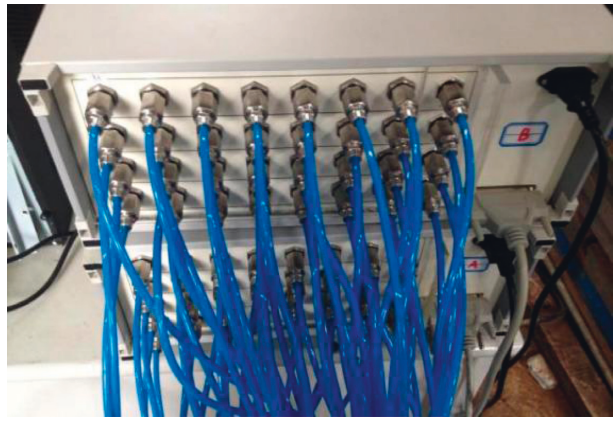

Figure 5: Multichannel pressure sensor integrated system.

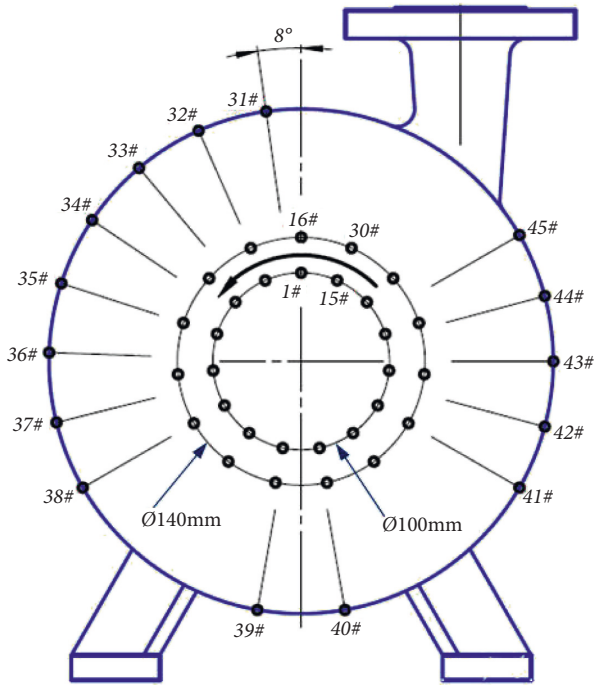

Figure 6: Arrangement diagram of pressure measurement point.

Table 1: Geometric coordinates of the circumferential pressure measurement point on cross-section of centrifugal pump volute.

No.	Angle (°)
31#	8
32#	24
33#	40
34#	56
35#	72
36#	88
37#	104
38#	120
39#	170
40#	190
41#	240
42#	255
43#	270
44#	285
45#	300

always higher than the experimental pump and the whole piping system, and the free liquid level in the tank is higher than the level of the pump inlet about 1.0 m.

2.4. Pressure Measurement Scheme. In this paper, we intend to conduct four different rotational speed conditions: low speed, moderate speed, above average speed, and high speed and select four to five flow condition points at various speeds for comparative study. The pressure measurement scheme in the experiment is shown in Table 2. Under the condition of low speed, moderate speed, above average speed, and high speed, five, five, four, and five working conditions would be measured. In the future work, more working conditions would be deeply studied so as to obtain more conclusions.

3. Experimental Results Analysis

3.1. Transient Pressure Pulsations. In order to more comprehensively analyze the instantaneous pressure pulsation on the wall of the volute casing of the centrifugal pump, this paper selects a flow condition for analysis in four rotational speed cases and at each speed, as shown in Table 3. At the same time for the instantaneous pressure pulsation, the magnitude of the pulsation can, to a certain extent, reflect the degree of fluid flow turbulence and hydraulic losses at the observed location and the use of instantaneous pressure fluctuations for better characterization of fluid flow and hydraulic losses [34]. The volatility is defined as follows:

$$C_A = \frac{(P_{\max} - P_{\min})}{P_{\max}}. \quad (1)$$

The real-time pressure fluctuations at the 1# and 16# pressure measurement points with radii of 50 mm and 70 mm, respectively, on the junction line between the second volute casing section and the front wall of the volute casing are shown in Figure 7 for the four scenarios of low, medium, above average, and high rotational speed. The pressure fluctuations at the 1#, 6#, and 11# pressure measurement points with radius of 50 mm and 16#, 21#, and 26# pressure measurement points with radius of 70 mm on the junction line between the second volute casing section and the solid wall surface of the leaf top clearance are shown in Table 4.

Under different working conditions, the instantaneous pressures at the pressure measurement points of 1# and 16# both show drastic fluctuation changes due to the rotation of the impeller. Despite the sharp fluctuations, the average value of pressure fluctuations is basically unchanged, which indicates that the pressure at the corresponding point is relatively stable. Under all conditions, the average pressure value of 16# pressure measurement points on the front wall of the volute casing is much larger than the pressure value of 1# measurement point on the inner ring, and the average pressure value of the outer ring is larger than the pressure value of the inner ring. With the increase of radius, the average pressure value of the front wall of the volute casing also increases. In addition, at the same pressure measurement point, its pressure value increases with the increase of pump shaft rotational speed. The pressure fluctuation at the same radius on the front wall of the volute casing varies, but the variation is not significant. In the three rotate speed conditions of low speed, middle speed, and above average speed, the pressure fluctuation amplitude is greater than 100% at the measurement points of 1#, 6#, and 10# because the minimum pressure value is less than 0. In addition, it is obvious to find that the pressure fluctuation on the front wall of the volute casing is significantly larger than the fluctuation on the inner ring, and the pulsation amplitude of pressure measurement points 1#, 6#, and 11#, which are closer to the impeller inlet, is more intense than that of pressure measurement points 16#, 21#, and 26#, which are closer to the impeller outlet. This may be related to the inlet flow.

Table 2: Test scheme.

	Defined state	Rotational speed (r/min)	Flow rate (m^3/h)											
			0.0	1.0	1.5	3.0	4.5	5.0	6.0	7.0	7.5	9.0	10.5	12.0	13.5
No. 1	Low speed	1450		√		√		√		√		√			
No. 2	Moderate speed	2000	√			√			√			√		√	
No. 3	Above average speed	2175			√		√				√		√		
No. 4	High speed	2900			√		√				√		√		√

Table 3: Specific working conditions.

State	Low speed	Moderate speed	Above average speed	High speed
Rotational speed (r/min)	1450	2000	2175	2900
Flow rate (m^3/h)	5.0	6.0	7.5	7.5

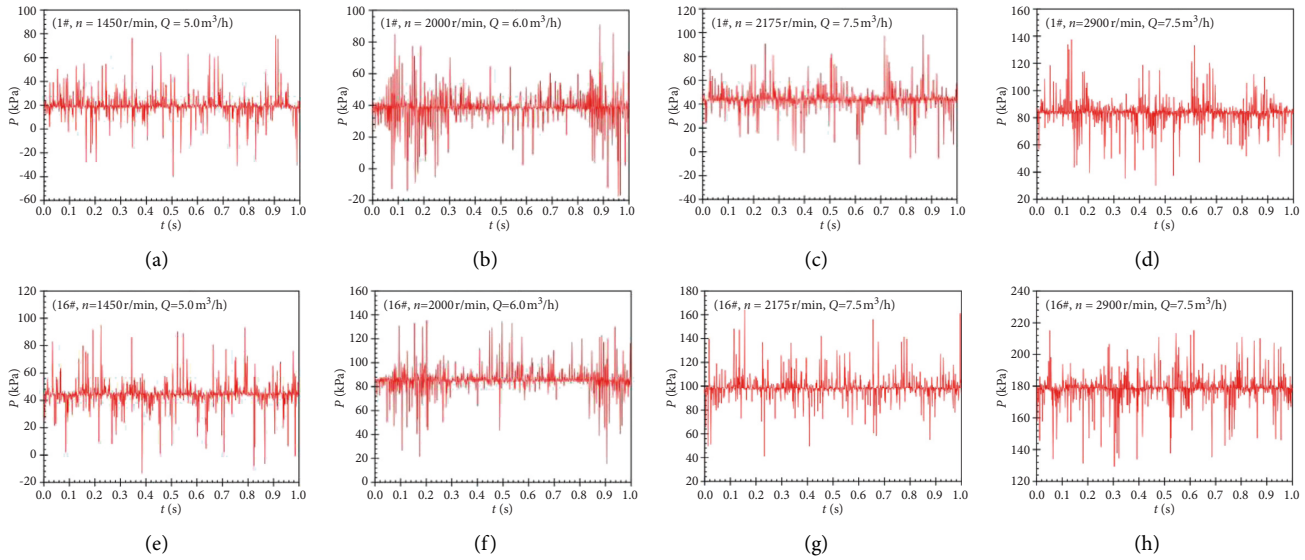

Figure 7: Variation characteristics of the instantaneous pressure at front wall of the volute casing.

Table 4: Pressure fluctuation of pressure measurement point on the front wall of the volute casing.

State	Rotational speed (r/min)	Flow rate (m^3/h)	Pressure fluctuation amplitude					
			1# (%)	6# (%)	11# (%)	16# (%)	21# (%)	26# (%)
Low speed	1450	5.0	150.86	148.58	158.13	113.97	107.14	113.88
Moderate speed	2000	6.0	118.94	107.50	128.74	88.44	72.74	82.43
Above average speed	2175	7.5	110.85	102.27	131.60	74.99	61.92	64.83
High speed	2900	7.5	78.11	79.84	81.37	39.85	39.68	41.67

Figure 8 shows the real-time pressure fluctuations at pressure measurement points 31#, 38#, 43#, and 45# on the junction line between the middle section and the inner section of the volute for four rotational speed conditions: low speed, medium speed, above average speed, and high speed. The pressure fluctuations at 31#, 38#, 43#, and 45# pressure measurement points on the junction line between the middle section and the inner section of the volute are shown in Table 5. And the specific angles corresponding to 31#, 38#, 43#, and 45# are shown in Table 1.

During the same working condition, the pressure values of pressure measurement points 43# and 45# near the exit side of the volute gear are obviously larger than those of pressure measurement points 31# and 38# on the other side, which may be due to the fact that the fluid flows out to the exit side of the volute gear with the direction of impeller rotation; in this process, part of the kinetic energy of the fluid is converted into static pressure energy, which leads to a higher static pressure value near the exit side of the volute shell than the other side. In addition, under different working conditions, it is obvious that with the increase of rotational speed, the static pressure value on the inner wall of the volute casing increases significantly, and the fluctuation magnitude also decreases gradually, for example, 31# pressure measurement point; the average static

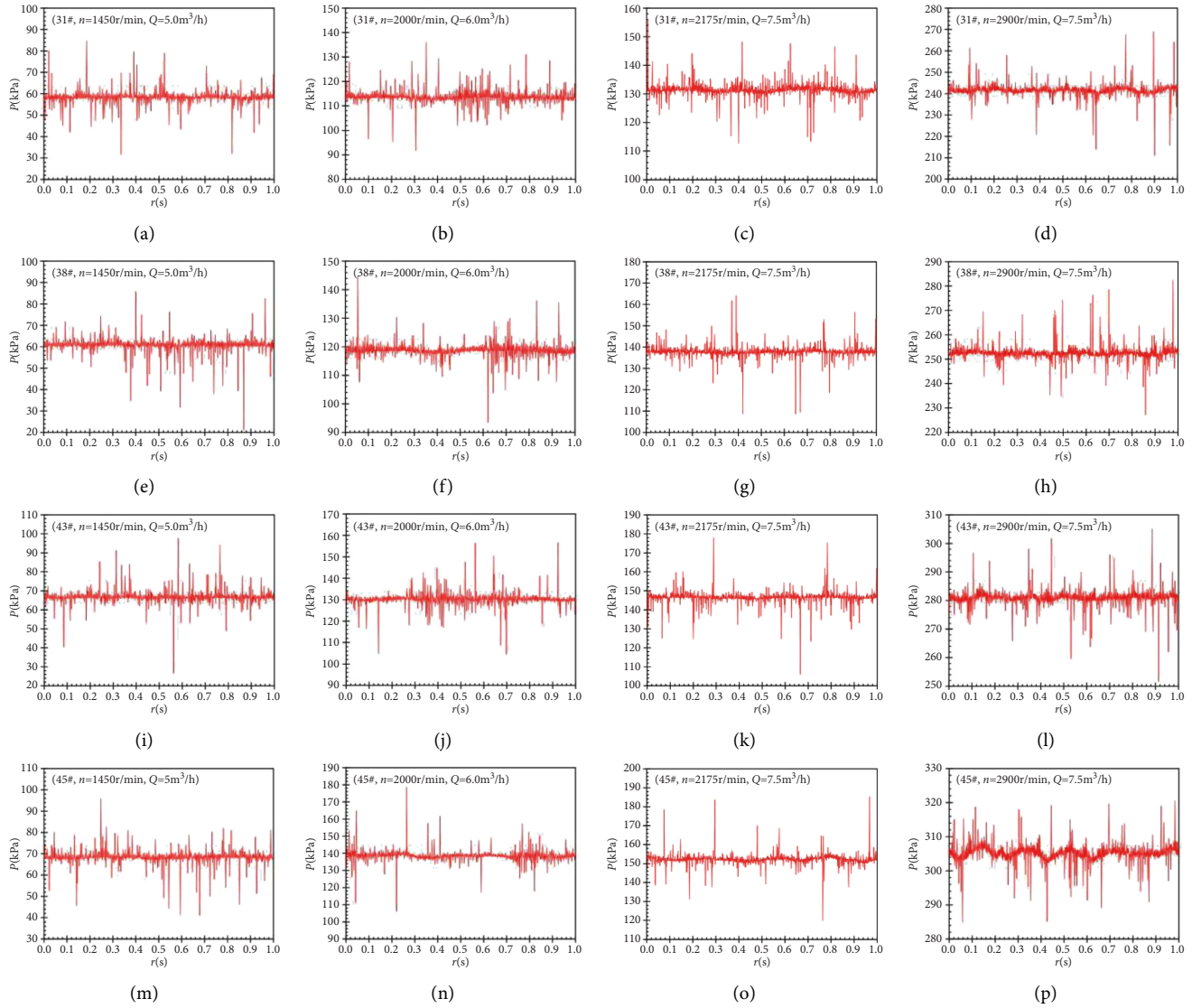

Figure 8: Variation characteristics of the instantaneous pressure on the middle section of the volute.

Table 5: Pressure fluctuation amplitude on the middle section of volute casing.

	Rotational speed (r/min)	Flow rate (m^3/h)	Pressure fluctuation amplitude			
			31# (%)	38# (%)	43# (%)	45# (%)
Low speed	1450	5.0	62.57	75.44	72.76	57.14
Moderate speed	2000	6.0	32.47	35.43	33.26	40.56
Above average speed	2175	7.5	27.60	33.72	40.42	35.27
High speed	2900	7.5	21.47	19.48	17.51	11.13

pressure value is only 58.384 kPa under 1450 r/min working condition; and the fluctuation magnitude reaches 62.57%, but when the rotational speed increases to 2900 r/min, the average static pressure value increased to 241.557 kPa and the fluctuation decreased to 21.47%. Therefore, the pressure pulsation on the inner section of the volute fluctuates drastically during the working process, but the average value of pressure fluctuation is basically unchanged; meanwhile, the average value of pressure fluctuation gradually increases and the magnitude of fluctuation gradually decreases with the increase of pump shaft speed.

3.2. Pressure Distribution at the Front Wall of Volute Casing. Figure 9 shows the average static pressure distribution at a diameter of 100 mm on the front wall of the volute casing for four speed conditions: low speed, medium speed, above average speed, and high speed. At any speed, for any pressure measurement point, the static pressure tends to decrease as the pump delivery flow increases. For example, for #1 pressure measurement point, at 1450 r/min, the average static pressure values at 5 steady flow conditions (1.0, 3.0, 5.0, 7.0, and 9.0 m^3/h) are 22.770 kPa, 21.261 kPa, 19.527 kPa,

17.058 kPa, and 14.665 kPa, respectively; at 2900 r/min, the average static pressure values at 5 steady flow conditions are 22.770 kPa, 21.261 kPa, 19.527 kPa, 17.058 kPa, and 14.665 kPa, respectively; at 2900 r/min, the average static pressure values at five steady flow conditions (1.5, 4.5, 7.5, 10.5, and 13.5 m^3/h) were 94.480 kPa, 89.817 kPa, 83.883 kPa, 77.237 kPa, and 69.693 kPa, respectively.

Theoretically, the static pressure in the direction of the same radius circumference should be approximately constant. However, the test results in Figure 9 show that the average static pressure value is not constant, but has certain fluctuation characteristics. For example, at a rotational speed of 1450 r/min and a steady flow rate of 1.0 m^3/h, the average static pressure values in the circumferential direction of the front wall of the volute casing with a diameter of 100 mm are 22.770 kPa, 21.023 kPa, 19.505 kPa, 21.903 kPa, 23.815 kPa, 22.914 kPa, 19.668 kPa, 22.7025 kPa, 23.066 kPa, 24.363 kPa, 24.418 kPa, 25.541 Pa, 24.962 kPa, 25.733 kPa, and 24.138 kPa. It was found by disassembling and testing the pump that this average static pressure fluctuation characteristic was mainly due to the different roughness differences caused by rust generated after long-term placement. Therefore, it is very important to improve the machining accuracy and reduce the wall roughness as much as possible to improve the pressure pulsation and pressure distribution in the pump. Meanwhile, the study of the effect of roughness or local envelope structure on pressure pulsation is one of the future works.

By comparison, it is found that the circumferential static pressure distribution law under different flow conditions at any speed has obvious differences. Such as rotational speed at 1450 r/min, in the small flow condition (1.0 m3/h), the static pressure value from 1# to 15# pressure measurement points generally shows the distribution characteristics of falling, rising, falling again, rising, and falling again; while in the large flow condition (9.0 m3/h), the static pressure value from 1# to 15# pressure measurement points generally shows overall distribution characteristics of rising and falling again. Differences in pressure distribution characteristics due to different working conditions are caused by changes in the volumetric efficiency of open impeller centrifugal pumps. It has been shown that the volumetric efficiency of centrifugal pumps varies depending on the working conditions. Since the impeller tested in this paper is an atypical open impeller, the gap leakage is more complicated, and the resulting volumetric efficiency varies with operating conditions. Therefore, it will be one of the future works to carry out the full 3D numerical calculation of this model pump and obtain the volumetric efficiency and internal pressure distribution under different working conditions by numerical calculation.

Figure 10 shows the average static pressure distribution at the diameter 140 mm on the front wall of the volute casing for four rotational speed conditions: low speed, middle speed, above average speed, and high speed. Compared with the average static pressure at 100 mm on the front wall of the volute casing, the average static pressure distribution characteristics at 140 mm also show some similar patterns. For example, in the same speed case, with the pump flow rate increases, the static pressure is showing a decreasing trend; the same radius circumferential direction of the average static pressure is not constant, but presents a certain degree of fluctuation characteristics.

For the pressure measurement points from 16# to 30#, in the case of rotational speed $n = 1450$ r/min, under the small flow condition (1.0 m^3/h), the pressure generally shows the distribution characteristics of falling, rising, and then falling; under the large flow condition (such as 9.0 m^3/h), the pressure generally shows the distribution characteristics of falling, rising, then falling, and then rising. The reason for the difference in pressure distribution law lies in two aspects: it may be a secondary factor, that is, due to the different local roughness in different directions, which needs to be confirmed and studied in depth. It should be the main factor; that is, $D = 100$ mm circumference is affected by inlet incoming flow, inlet return flow, and inlet leakage, while $D = 140$ mm circumference is affected by outlet return flow and outlet leakage. Obviously, for giving this atypical open impeller, its leaf top clearance leakage is very complicated. Therefore, in the subsequent work, the numerical calculation to obtain the detailed internal leakage law and pressure characteristics and other nonconstant flow characteristics is very necessary and need to explore in depth the work content.

3.3. Pressure Pulsation Intensity of Volute Casing. Due to the dynamic and static interference effect of the rotating and stationary parts of the centrifugal pump, the flow field inside the centrifugal pump will show nonconstant disturbance flow characteristics. This perturbed flow will cause pressure pulsation in the flow field, and the fluid will transfer the pressure pulsation to the impeller and volute gear, triggering vibration, and noise of the centrifugal pump. Therefore, the analysis of the pressure pulsation can effectively show the degree of fluid flow drastic. In this paper, the pressure coefficient is used to dimensionless the transient pressure, and the calculation formula is defined as follows:

$$C_p = \frac{p - \overline{p}}{(1/2)\rho U_2^2}, \tag{2}$$

where U_2 is the impeller outlet circumferential velocity, m/s; p is the transient static pressure, Pa; $\overline{p}$ is the average static pressure, Pa; and ρ is the density of water, kg/m^3.

For the degree of pressure pulsation within the centrifugal pump, the analysis is performed using the pressure pulsation intensity C_{psd}, and the calculation formula is defined as follows:

$$C_{psd} = \frac{\sqrt{(1/N)\sum_{i=0}^{N-1}\left(p\left(x,y,z,t_i\right) - (1/N)\sum_{i=0}^{N} p\left(x,y,z,t_i\right)\right)}}{(1/2)\rho U_2^2} = \frac{\sqrt{(1/N)\sum_{i=0}^{N-1}\left(p - \overline{p}\right)}}{(1/2)\rho U_2^2}, \tag{3}$$

where $p(x, y, z, t_i)$ denotes the static pressure corresponding to each time step and N is the number of time steps in the pulsation cycle.

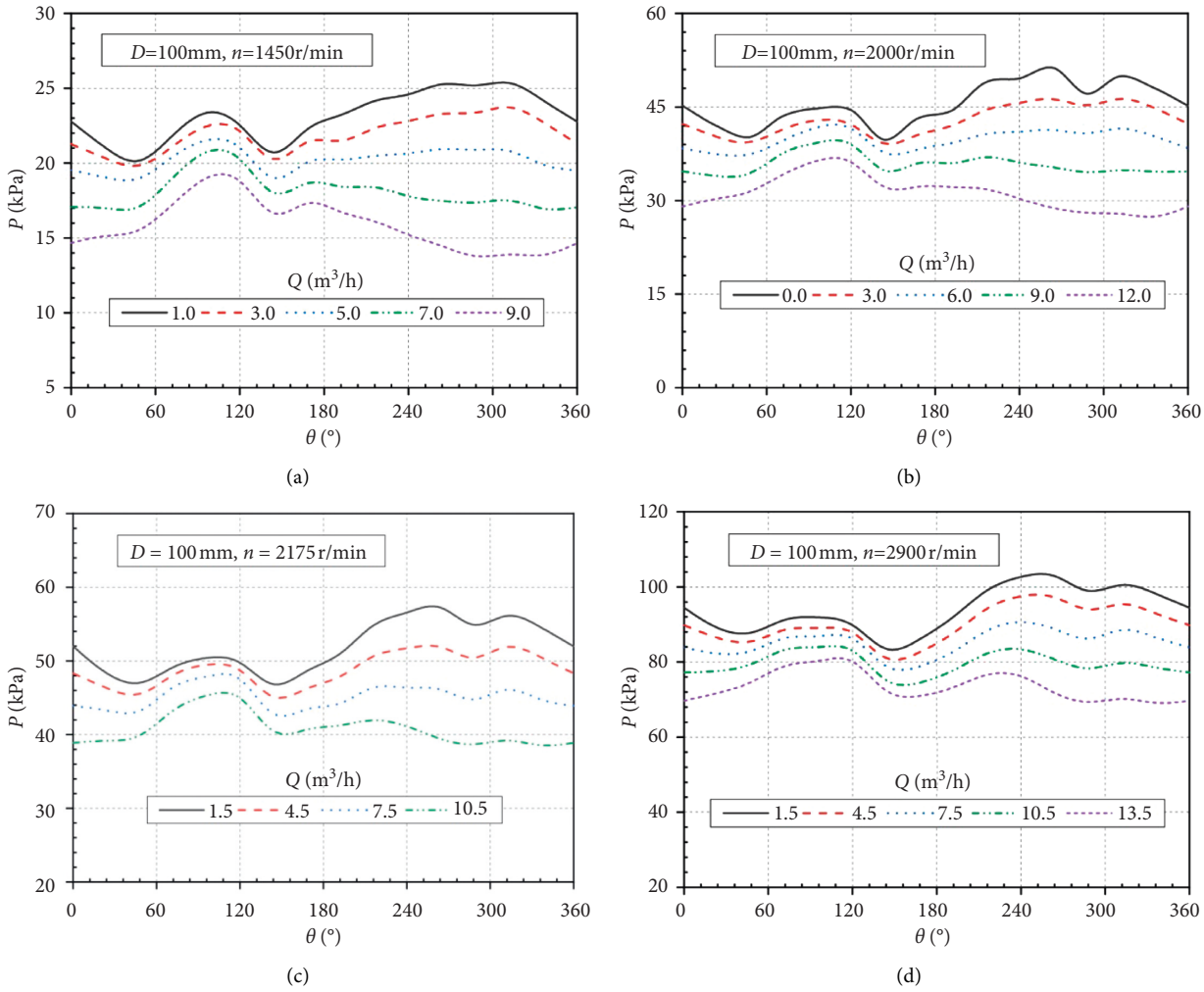

Figure 9: Average static pressure distribution at the front wall of volute casing ($D = 100$ mm).

The pressure pulsation intensity at different locations on the circumference of $D = 100$ mm diameter on the front wall of the volute casing under four rotational speed conditions, namely, low speed, medium speed, above average speed, and high speed, is shown in Figure 11. The minimum pressure pulsation strength appears at the junction of the fifth section and the front wall of the volute casing in each speed condition, and its strength varies with the change of speed, and the minimum strengths are 0.11, 0.057, 0.048, and 0.0265 for low, medium, above average, and high rotational speed conditions. At the same time, the trend of pressure monitoring points on the circumference at the same speed condition varies somewhat at different flow rates. For example, at a rotational speed of 1450 r/min and a small flow rate (1.0 m^3/h), the pressure pulsation intensity of the measurement points from 1# to 15# generally showed the characteristics of falling, rising, falling again, rising again, and in falling and rising again distribution; while at a large flow rate (9.0 m^3/h), the pressure pulsation intensity of the measurement points from 1# to 15# generally showed the characteristics of falling, rising, falling again, rising again, then fall, then rise, then fall, and then rise again distribution characteristics. Under the other working conditions, the distribution characteristics of pressure pulsation intensity on the circumference are basically consistent with the low rotational speed working condition.

Figure 12 shows the pressure pulsation intensity at a diameter of $D = 140$ mm on the front wall of the volute casing during four rotational speeds: low speed, medium speed, above average speed, and high speed. Compared with the pressure pulsation intensity at $D = 100$ mm on the front wall of the volute casing, there are some similar patterns. For example, the pressure pulsation intensity at each point in the circumferential direction shows a tendency to become smaller as the speed increases. The pressure pulsation intensity in the circumferential direction of the same radius is not constant, but shows a certain degree of fluctuation characteristics.

However, the location of the minimum pressure pulsation intensity was changed from the junction of the fifth section with the front wall of the volute casing to the fourth section. The reason for the above change may be consistent with the reason for the difference of the average static pressure at different diameters, and both need to further reduce the error in the subsequent study.

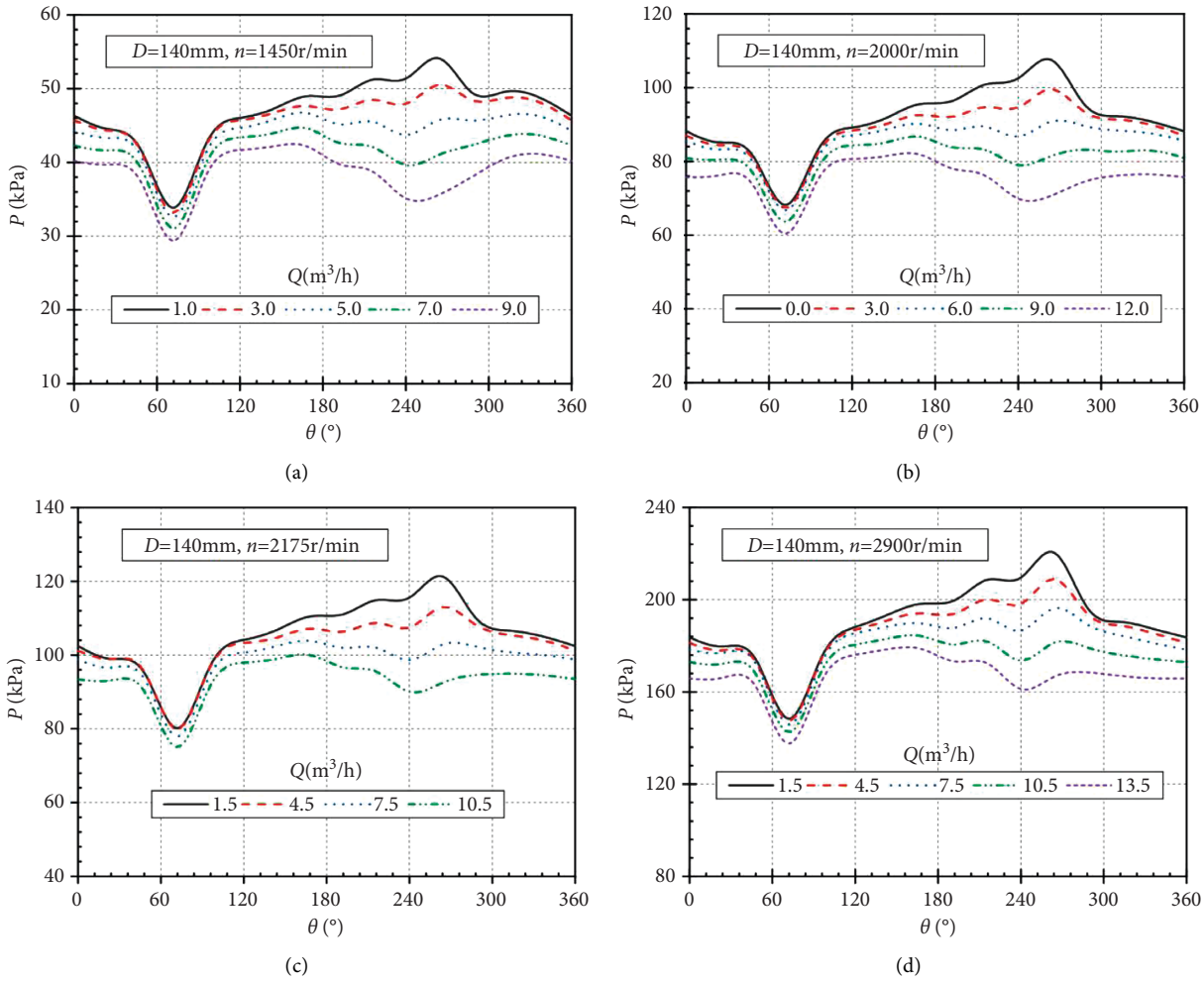

Figure 10: Average static pressure distribution at the front wall of volute casing ($D = 140$ mm).

3.4. Circumferential Pressure Distribution of Volute Casing. Figure 13 shows the average static pressure distribution in the circumferential direction of the middle section of the volute for four rotational speed cases: low speed, medium speed, above average speed, and high speed. It can be found that, in the same speed case, with the increase of pump delivery flow, the static pressure shows a decreasing trend, which is also in line with the general hydrodynamic law of the pump. For example, for 45# pressure measurement point, in the case of speed 1450 r/min, the average static pressure values of 5 stable flow conditions (1.0, 3.0, 5.0, 7.0, and 9.0 m^3/h) are 82.123 kPa, 79.152 kPa, 68.421 kPa, 51.716 kPa, and 30.133 kPa, respectively; in the case of speed 2000 r/min, the average static pressure of 5 stable flow conditions (1.0, 3.0, 5.0, 7.0, and 9.0 m^3/h) are 82.123 kPa, 79.152 kPa, 68.421 kPa, 51.716 kPa, and 30.133 kPa, respectively. The average hydrostatic pressure values for the five steady flow conditions (0.0, 3.0, 6.0, 9.0, and 12.0 m^3/h) at 2000 r/min were 159.395 kPa, 155.255 kPa, 138.563 kPa, 108.235 kPa, and 64.781 kPa, respectively; at a speed of 2175 r/min, the average hydrostatic pressure values for the four steady flow conditions (1.5, 4.5, 7.5, and 10.5 m^3/h) were 183.967 kPa, 176.901 kPa, 152.267 kPa, and 116.640 kPa, respectively; at a speed of 2900 r/min, the average hydrostatic pressure values for the five steady flow conditions (1.5, 4.5, 7.5, 10.5, and 13.5 m^3/h) were 332.062 kPa, 326.071 kPa, 305.137 kPa, 265.328 kPa, and 216.364 kPa, respectively.

Meanwhile, it can be found that the average static pressure is basically constant and does not change significantly in the counterclockwise flow direction from the second section (0°) to the sixth section (180°) of the volute shell under the four speed cases. For example, in the case of speed 1450 r/min and flow rate 1.0 m^3/h (small flow rate condition), the average static pressure values of pressure measurement points 31#~39#, which located at middle section of the volute and in the circumferential direction of the inner wall of volute, are 61.140 kPa, 61.787 kPa, 62.055 kPa, 61.669 kPa, 63.711 kPa, 62.501 kPa, 61.959 kPa, 62.935 kPa, and 62.225 kPa. However, after the sixth section (180°) from the volute shell, the average static pressure distribution pattern appears significantly different at different working flow rates. In the middle- and small-sized flow conditions, the average static pressure shows a monotonic gradually rising trend; in the large flow conditions, the average static pressure shows a trend of falling and then rising; that is, there is a local minimum value, and the

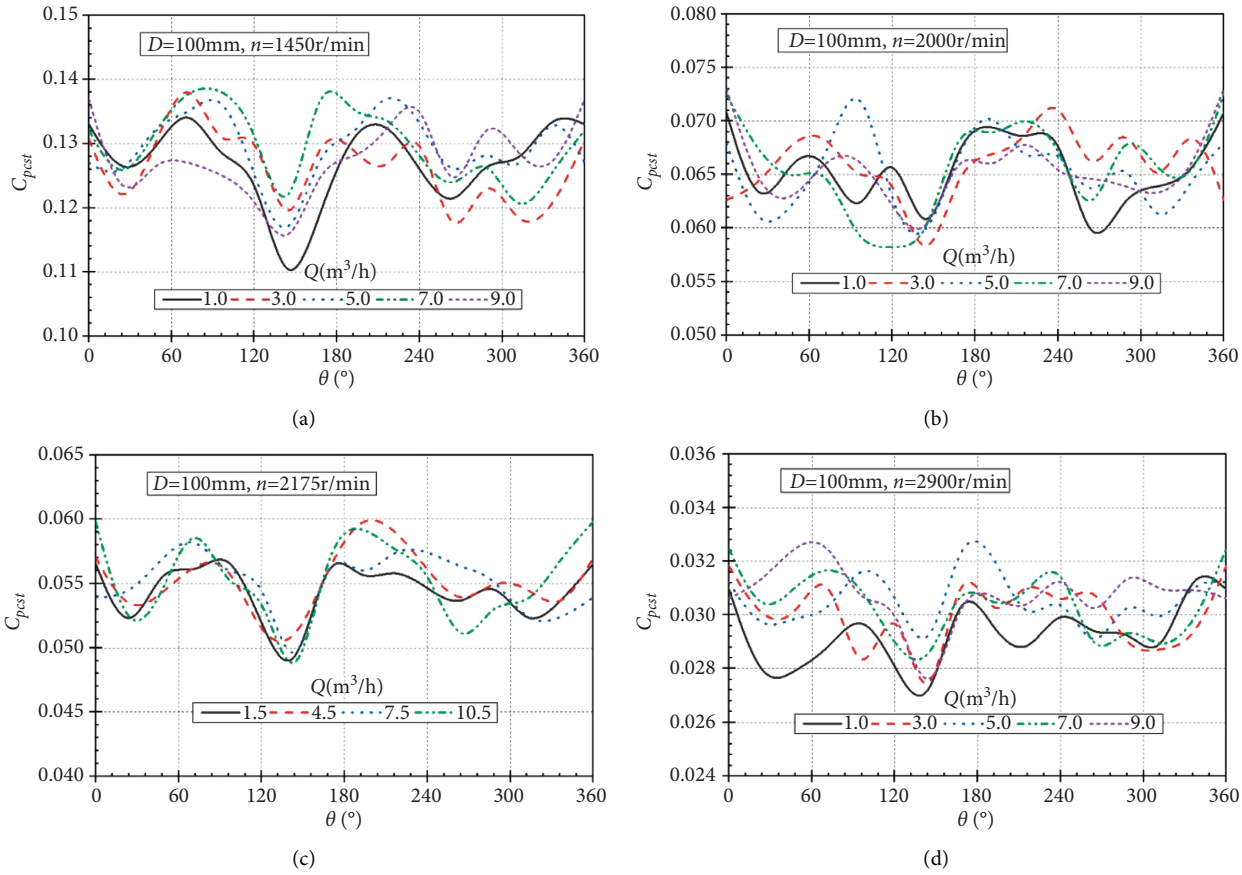

Figure 11: Pressure pulsation intensity of at the front wall of volute casing ($D = 100$ mm).

location is 44# pressure measurement point. For the pressure measurement point 44#, the minimum static pressure values for five steady flow conditions (1.0, 3.0, 5.0, 7.0, and 9.0 m^3/h) were 81.320 kPa, 73.731 kPa, 68.421 kPa, 28.327 kPa, and −7.387 kPa at a speed of 1450 r/min, and the minimum static pressure values for five steady flow conditions (0.0, 3.0, 6.0, 9.0, and 12.0 m3/h) were 157.839 kPa, 149.0 kPa, and −7.387 kPa at a speed of 2000 r/min; the minimum static pressure values for the five steady flow conditions (0.0, 3.0, 6.0, 9.0, and 12.0 m^3/h) were 157.839 kPa, 149.662 kPa, 118.041 kPa, 68.074 kPa, and −9.512 kPa, respectively; minimum static pressure values for four steady flow conditions (1.5, 4.5, 7.5, and 10.5 m^3/h) were 181.768 kPa, 164.331 kPa, 121.787 kPa, and 63.144 kPa at a speed of 2175 r/min; and at a speed of 2900 r/min, the minimum static pressure values for the five steady flow conditions (1.5, 4.5, 7.5, 10.5 and 13.5 m^3/h) were 327.695 kPa, 312.999 kPa, 271.498 kPa, 205.552 kPa, and 124.037 kPa, respectively. This indicates that for the current snail casing, the pressure at the measurement point 44# is the lowest at the position slightly after the eighth section. It also shows that the geometric parameters at the 44# measurement point at this location are small, which leads to a sharp increase in flow rate when the flow rate increases, resulting in a sudden drop in pressure. Under high flow conditions, the flow velocity here increases sharply; it is known that the hydraulic loss is proportional to the square of the flow velocity; therefore, the high flow conditions here will cause a huge pressure loss, which will affect the changing characteristics of the pump head, and will easily cause a sudden drop in the pump head at high flow rates. Therefore, to avoid the phenomenon of head plunge and to expand the working range of this test pump, the geometry at 44# needs to be enlarged.

3.5. Standard Deviations. The standard deviation describes the average of the distances from the mean for each data set and is denoted by σ. The standard deviation reflects the degree of dispersion of a data set; the smaller the standard deviation, the less these values deviate from the mean, and vice versa. The magnitude of the standard deviation can be measured by the relationship between the standard deviation and the multiplicity of the mean. The overall standard deviation is the experimental standard deviation in the case of infinite number of measurements, also known as the theoretical standard deviation. The calculation formula is defined as follows:

$$\sigma = \sqrt{\frac{1}{n}\sum_{i=1}^{n}(x_i - \mu)^2}, \tag{4}$$

where μ represents the mean value of the test data samples.

Figure 14 shows the standard deviation plot for the 290 r/min case. It can be seen that the standard deviation basically fluctuates in the interval [7, 10] on the front wall of the

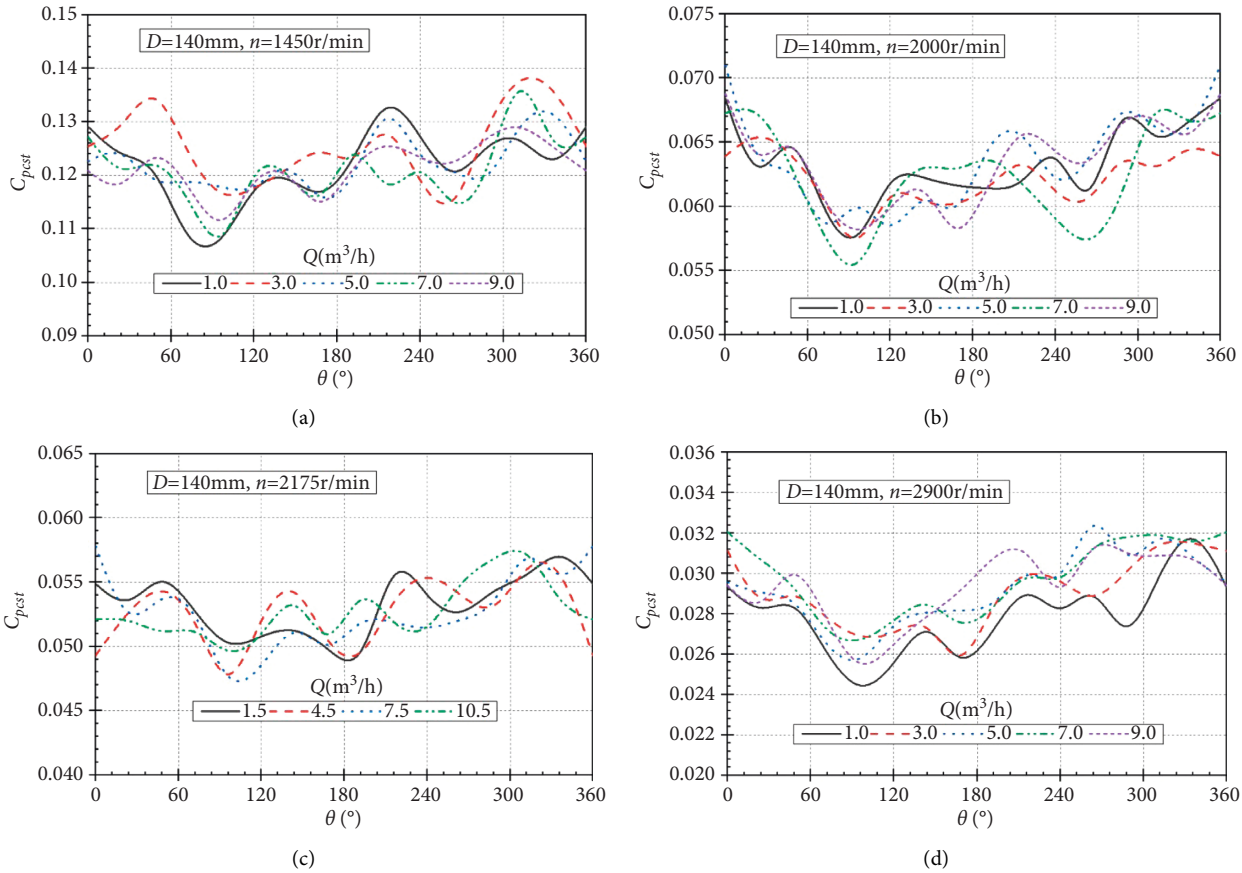

Figure 12: Pressure pulsation intensity of at the front wall of volute casing ($D = 140$ mm).

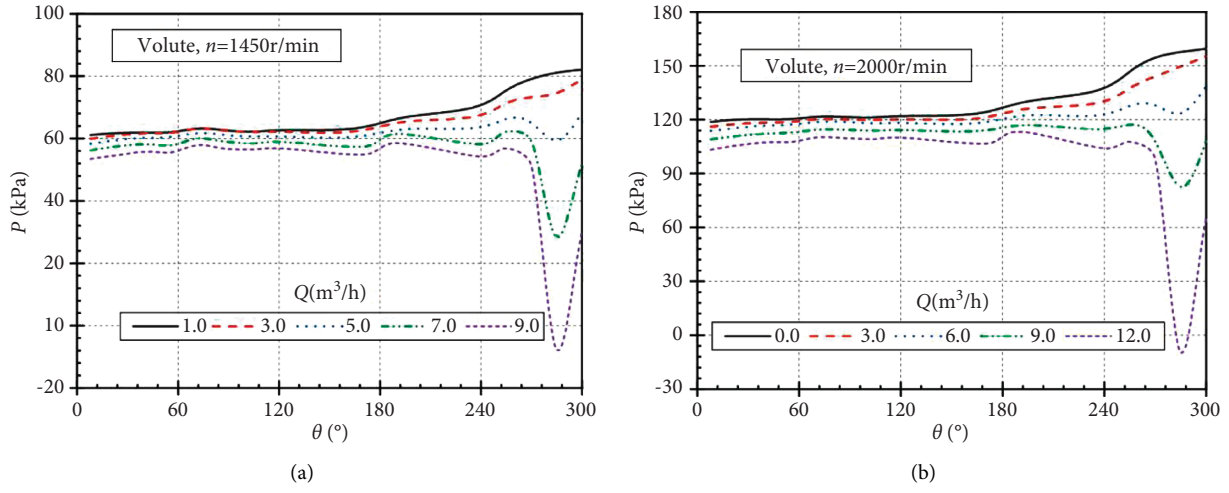

Figure 13: Continued.

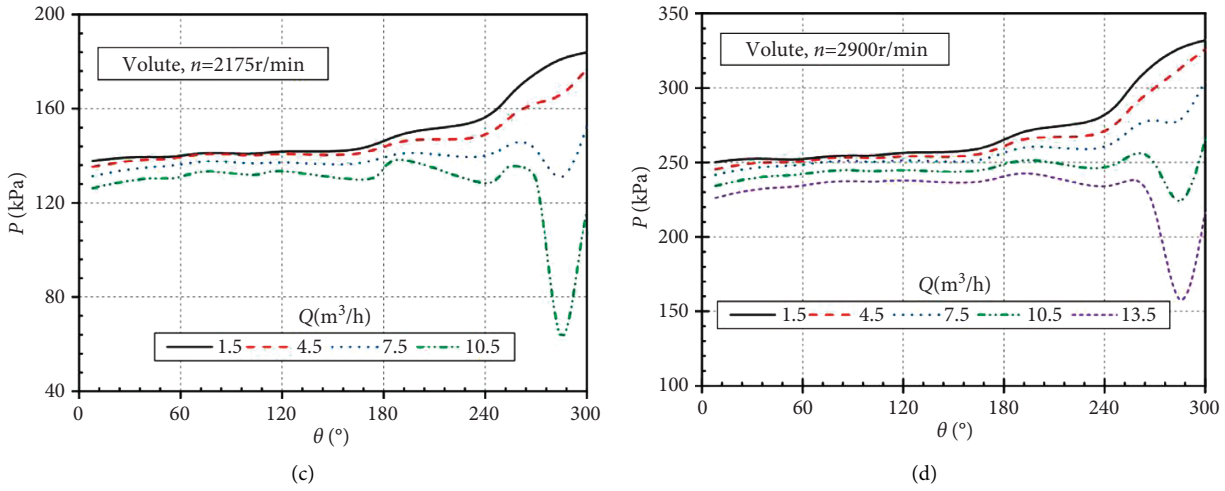

Figure 13: Circumferential average static pressure distribution at the middle section of volute.

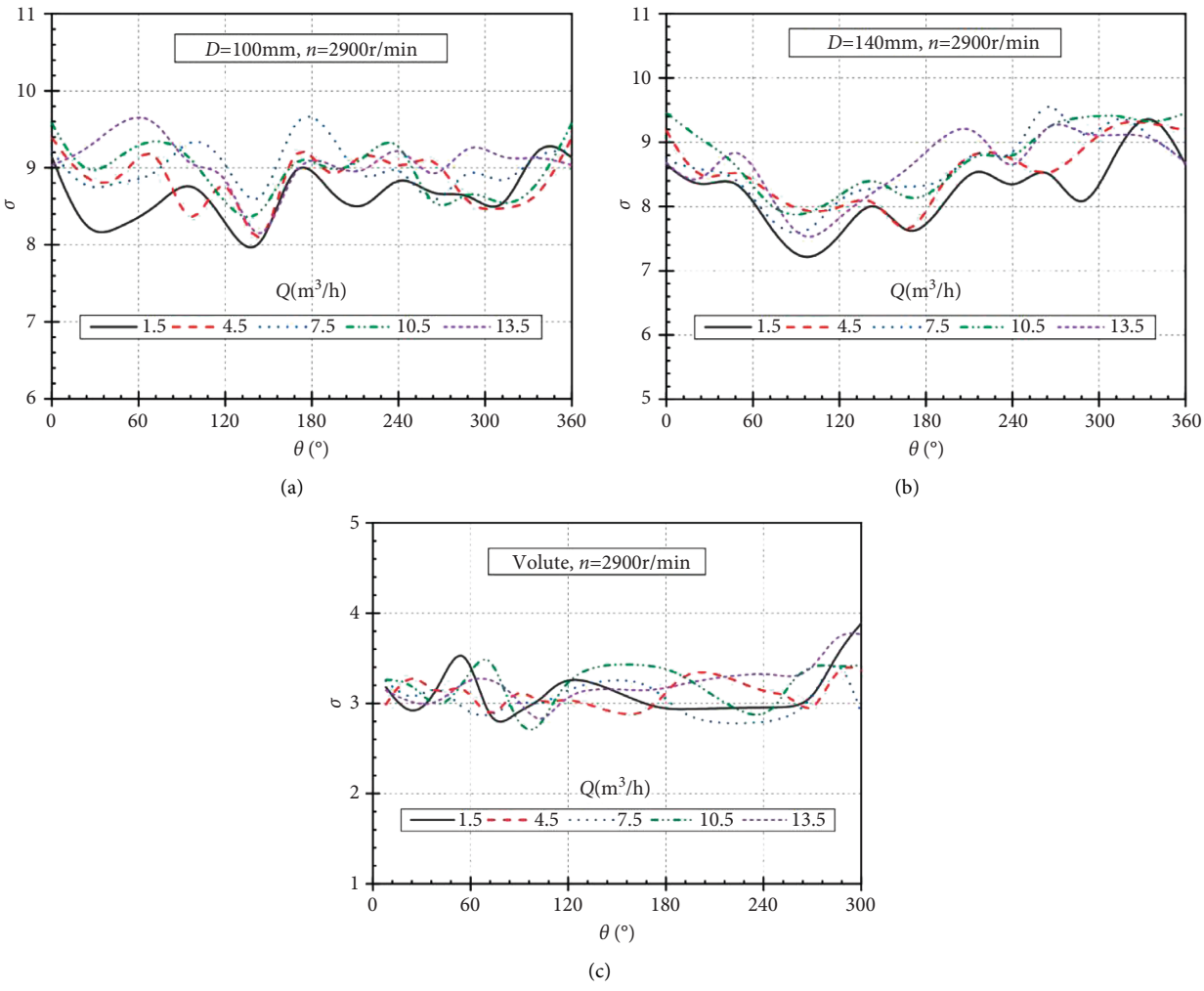

Figure 14: Standard deviation distribution.

volute casing ($D = 100$ mm and $D = 140$ mm), while it fluctuates in the interval [2.6, 3.8] for the inner section of the volute. This fully indicates that the pressure pulsation in the front wall of this model pump is very huge and the flow is extremely complicated; while on the inner section of the volute, the pressure pulsation is relatively small.

4. Conclusions

The instantaneous pressure pulsation on the inner section of volute fluctuates more sharply during the pump operation, and the closer pressure pulsation is more sharply to the outlet of the volute shell; after increasing the pump shaft speed, the fluctuation amplitude gradually decreases. In the second section to the sixth section of the volute casing, the average static pressure is basically constant; after the sixth section of the volute casing, the average static pressure distribution pattern varies significantly according to the working conditions. The pressure pulsation on the front wall of volute casing differs depending on the position and working condition, and the pressure pulsation on the front wall of volute casing is more intense than that on the inner section of volute; affected by the roughness of the wall and the leakage of the top clearance, the static pressure in the direction of the same radius circumference shows nonconstant characteristics; the intensity of the pressure pulsation on t the front wall of volute casing decreases with the increase of the rotational speed, and the higher the rotational speed, the less intense the pressure pulsation.

Data Availability

The data used to support the findings of this study are available from the corresponding author upon request.

Conflicts of Interest

The authors declared they have no potential conflicts of interest with respect to the research, authorship, and/or publication of this article.

Acknowledgments

The research was financially supported by the "Pioneer" and "Leading Goose" R & D Program of Zhejiang (Grant no. 2022C03170), National Natural Science Foundation of China (Grant no. 51876103), and Zhejiang Provincial Natural Science Foundation of China (Grant nos. LZY21E060001 and LZY21E060002).

References

[1] Q. Si, S. Yuan, J. Yuan, and L. Tong, "Effect of interaction between blade and volute tongue of centrifugal pumps on the performance and pressure pulsation," *Fluid Machinery*, vol. 40, no. 6, pp. 22–26, 2012.

[2] R. Spence and J. Amaral-Teixeira, "Investigation into pressure pulsations in a centrifugal pump using numerical methods supported by industrial tests," *Computers & Fluids*, vol. 37, no. 6, pp. 690–704, 2008.

[3] J. L. Parrondo-Gayo, J. Gonzalez-Perez, and J. Fernandez-Francos, "The effect of the operating point on the pressure fluctuations at the blade passage frequency in the volute of a centrifugal pump," *Journal of Fluids Engineering*, vol. 124, no. 3, pp. 784–790, 2002.

[4] A. E. Khalifa, A. M. Al-Qutub, and R. Ben-Mansour, "Study of pressure fluctuations and induced vibration at blade-passing frequencies of a double volute pump," *Arabian Journal for Science and Engineering*, vol. 36, no. 7, pp. 1333–1345, 2011.

[5] H. Wang and H. Tsukamoto, "Experimental and numerical study of unsteady flow in a diffuser pump at off-design conditions," *Journal of Fluids Engineering*, vol. 125, no. 5, pp. 767–778, 2003.

[6] Z. Yao, F. Wang, L. Qu, R. Xiao, C. He, and M. Wang, "Experimental investigation of time-frequency characteristics of pressure fluctuations in a double-suction centrifugal pump," *Journal of Fluids Engineering*, vol. 133, no. 10, 2011.

[7] Z. Wang, Z. Qian, J. Lu, and P. Wu, "Effects of flow rate and rotational speed on pressure fluctuations in a double-suction centrifugal pump," *Energy*, vol. 170, pp. 212–227, 2019.

[8] L. Zheng, X. Chen, H. S. Dou, W. Zhang, Z. Zhu, and X. Cheng, "Effects of clearance flow on the characteristics of centrifugal pump under low flow rate," *Journal of Mechanical Science and Technology*, vol. 34, no. 1, pp. 189–200, 2020.

[9] N. Zhang, M. Yang, B. Gao, Z. Li, and D. Ni, "Experimental investigation on unsteady pressure pulsation in a centrifugal pump with special slope volute," *Journal of Fluids Engineering*, vol. 137, no. 6, 2015.

[10] N. Zhang, M. Yang, B. Gao, Z. Li, and D. Ni, "Unsteady pressure pulsation and rotating stall characteristics in a centrifugal pump with slope volute," *Advances in Mechanical Engineering*, vol. 2014, Article ID 710791, 11 pages, 2014.

[11] N. Zhang, M. Yang, B. Gao, Z. Li, D. Ni, and H. Wang, "Experimental study on pressure fluctuation spectrum characteristics of low specific speed centrifugal pump," *Journal of Engineering and Thermophysics*, vol. 38, no. 9, pp. 1872–1876, 2017.

[12] Z. Yao, F. Wang, R. Xiao, H. Yan, Z. Liu, and M. Wang, "Key issues in pressure fluctuation experiments for centrifugal pumps," *Journal of Drainage and Irrigation Machinery Engineering*, vol. 28, no. 3, pp. 219–223, 2010.

[13] X. Zhao, Y. Xiao, Z. Wang, Y. Luo, and L. Cao, "Unsteady flow and pressure pulsation characteristics analysis of rotating stall in centrifugal pumps under off-design conditions," *Journal of Fluids Engineering*, vol. 140, no. 2, 2018.

[14] C. Wang, T. Zhang, X. Yang, H. Peng, and L. Dong, "Numerical simulation and performance prediction of positive and negative internal flow field of double suction pump," *Journal of Drainage and Irrigation Machinery Engineering*, vol. 33, no. 7, pp. 577–582, 2015.

[15] J. Chen, Y. Wang, H. Liu, C. Shao, and X. Zhang, "Internal flow and unsteady characteristics of ultra-low specific speed centrifugal pump," *Journal of Drainage and Irrigation Machinery Engineering*, vol. 36, no. 5, pp. 377–383, 2018.

[16] S. Yuan, Y. He, J. Yuan, X. Cong, and B. Zhao, "PIV measurement and numerical simulation of the internal flow field in centrifugal pump impeller with splitter blade," *Chinese Journal of Mechanical Engineering*, vol. 42, no. 5, pp. 60–63, 2006.

[17] W. Shi, L. Zhang, B. Chen, and T. Jiang, "Influence of gap on pressure pulsation and radial force of centrifugal pumps," *Journal of Drainage and Irrigation Machinery Engineering*, vol. 30, no. 3, pp. 260–264, 2012.

[18] X. Chen, L. Cao, P. Yan, P. Wu, and D. Wu, "Effect of meridional shape on performance of axial-flow fan," *Journal of Mechanical Science and Technology*, vol. 31, no. 11, pp. 5141–5151, 2017.

[19] S. Yang, X. Chen, D. Wu, and P. Yan, "Dynamic analysis of the pump system based on MOC–CFD coupled method," *Annals of Nuclear Energy*, vol. 78, pp. 60–69, 2015.

[20] D. Wu, P. Yan, X. Chen, and S. Yang, "Effect of trailing-edge modification of a mixed-flow pump," *Journal of Fluids Engineering*, vol. 137, no. 10, Article ID 101205, 2015.
[21] Y. Liu and L. Tan, "Spatial-temporal evolution of tip leakage vortex in a mixed flow pump with tip clearance," *Journal of Fluids Engineering*, vol. 141, no. 8, 2019.
[22] M. Liu, L. Tan, and S. Cao, "Influence of geometry of inlet guide vanes on pressure fluctuations of a centrifugal pump," *Journal of Fluids Engineering*, vol. 140, no. 9, 2018.
[23] W. Sun and L. Tan, "Cavitation-vortex-pressure fluctuation interaction in a centrifugal pump using bubble rotation modified cavitation model under partial load," *Journal of Fluids Engineering*, vol. 142, no. 5, 2020.
[24] W. Xiao and L. Tan, "Design method of controllable velocity moment and optimization of pressure fluctuation suppression for a multiphase pump," *Ocean Engineering*, vol. 220, pp. 108402–108413, 2021.
[25] K. Luo, Y. Wang, H. Liu, J. Chen, Y. Li, and J. Yan, "Effect of suction chamber baffles on pressure fluctuations in a low specific speed centrifugal pump," *Journal of Vibroengineering*, vol. 21, no. 5, pp. 1441–1455, 2019.
[26] L. Bai, L. Zhou, C. Han, Y. Zhu, and W. Shi, "Numerical study of pressure fluctuation and unsteady flow in a centrifugal pump," *Processes*, vol. 7, no. 6, p. 354, 2019.
[27] N. Zhang, J. Jiang, B. Gao, and X. Liu, "DDES analysis of unsteady flow evolution and pressure pulsation at off-design condition of a centrifugal pump," *Renewable Energy*, vol. 153, pp. 193–204, 2020.
[28] B. Cui, Y. Zhang, and Y. Huang, "Analysis of the pressure pulsation and vibration in a low-specific-speed centrifugal pump," *Journal of Fluids Engineering*, vol. 143, no. 2, 2021.
[29] C. Wu, W. Zhang, P. Wu et al., "Effects of blade pressure side modification on unsteady pressure pulsation and flow structures in a centrifugal pump," *Journal of Fluids Engineering*, vol. 143, no. 11, 2021.
[30] Y. Zeng, Z. Yao, R. Tao, W. Liu, and R. Xiao, "Effects of lean mode of blade trailing edge on pressure fluctuation characteristics of a vertical centrifugal pump with vaned diffuser," *Journal of Fluids Engineering*, vol. 143, no. 11, 2021.
[31] C. Wu, Q. Li, F. Zheng et al., "Improve of unsteady pressure pulsation based on jet–wake suppression for a low specific centrifugal pump," *Journal of Fluids Engineering*, vol. 143, no. 11, 2021.
[32] Y. Zhang, Z. Zhu, Y. Jin, B. Cui, Y. Li, and H. Dou, "Experimental study on a centrifugal pump with an open impeller during startup period," *Journal of Thermal Science*, vol. 22, no. 1, pp. 1–6, 2013.
[33] Y. Zhang, Z. Zhu, and W. Li, "Experiments on pressure distribution of a low specific-speed centrifugal pump with atypical open impeller," *Journal of Chemical Engineering of Japan*, vol. 53, no. 6, pp. 237–245, 2020.
[34] R. Zhu, B. Su, A. Yang, Q. Fu, and X. Wang, "Analysis of pressure pulsation characteristics of centrifugal pump," *Transactions of the Chinese Society for Agricultural Machinery*, vol. 41, no. 11, pp. 43–47, 2010.